Numerical investigations on ricochet of a spin-stabilised projectile on armour steel plates

Marina Seidl, Thomas Wolf, Rainer Nuesing

ISL - French-German Research Institute of Saint-Louis, 5 Rue du Général Cassagnou, 68300 Saint-Louis

Abstract

Expanding urbanisation poses new challenges. Developing countries are facing a rapid Urbanisation with an estimated 4.3 billion urban inhabitants by 2035 [1]. History has shown that conflict and large-scale disasters are likely to occur where large populations reside [2]. During peace-keeping missions, soldiers move in closed urban locations surrounded by house walls and close to their armoured vehicles. In event of combat, the likelihood of projectiles ricocheting in a closed environment—than on the open battlefield—arises. This study examines projectile ricochet, which is the deflection off a surface of a projectile from its original trajectory after striking the target at a low angle [3], with focus on the influence of the yaw angle α_t on the projectile behaviour after ricocheting. Numerical simulations—using the explicit Lagrangian solver—are used for a qualitative investigation, as measurement precision limits the determination of the influence of αt.

Keywords: Ricochet, spin-stabilised projectile, Finite Element (FE) Method, High velocity impact, Lagrangian method

1 Introduction

In the first half of the 19th century, first cylindrical-conical bullets were developed to be launched by standard infantry rifle. However, they tend to show that their orientation would not remain along the inertial axis (Fig. 1), which causes to set the bullet progressively against its trajectory and meet increasingly air resistance, which would lead to an unpredictable the bullet movement [1].

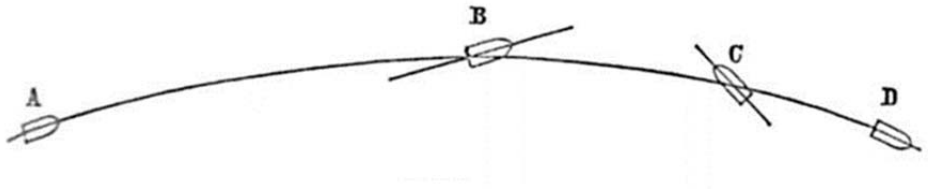

Fig. 1 Bullet trajectory without stabilisation [4]; A) bullet after launch; B) orientation not on inertial axis; C) increasing air resistance (bullet overturns); D) erratic bullet movement and imprecise

In order to gain a better performance, groves were added at the back of the bullet. That moved the resistance of air behind its centre of gravity (*COG*). Further advancements in gun powders enabled the development of elongated projectiles from the previous cylindrical-conical shaped bullets. Also being a proportionally longer, these projectiles had a smaller diameter (the calibre) with the same sectional density as a larger one can be driven at higher velocities. This resulted a longer maximum range, flatter trajectory, and greater penetrating power, all while reducing ammunition weight [4], and better propellants allowed greater muzzle velocities for bullets [5]. Advances in aerodynamics led to the pointed bullet. These bullets flew for greater distances more accurately and carried more energy with them. Pointed projectiles combined with machine guns increased the lethality in battle [6].
In order to keep bullets stable during their flight, two methods can be employed. Either projectiles achieve stability by forcing their centre of pressure (*CP*) behind their *COG* with tail surfaces, which was similarly achieved with grooves for shorter bullets. The CP behind the *COG* condition achieves stable projectile flight. The projectile will not overturn during flight through the atmosphere due to

aerodynamic forces. The second method spins the projectile around its rotational axis in order to stabilise them.

2 Spin-stabilised projectiles

Projectiles have their CP in front of their CG, which destabilizes them during flight. When launched, grooves inside the gun barrel give them an initial spin around their length or rotational axis, which stabilises them during the flight phase. The spinning mass creates gyroscopic forces that keep the projectile length axis resistant to the destabilizing overturning torque of the CP being in front of the CG [7].

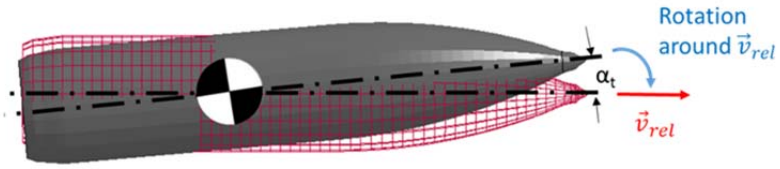

Fig. 2 Projectile angle of attack αt rotation around relative velocity vector $\vec{v}_{rel}$

Ideally, projectiles should rotate around their rotational axis, but in reality they rotate with yaw angle αt contained between the projectile axis and the relative velocity vector $\vec{v}_{rel}$ (Fig. 2).

Because the trajectory is not straight, but goes in an arch and also gravity acts on the projectile, its nose always tends to be slightly above the tangent to the trajectory. As the projectile spins, the rotational force upward on the nose causes the nose to lean to the right and this rightward cant causes what is called drift or spin drift [8]. Spin drift is defined as the phenomenon that occurs when a bullet fired through a barrel with a right-hand twist has a rotation that causes it to spin subtly to the right of the target (or to the left of the target when shot from a left-hand twist barrel) [9]

The aerodynamic forces pushing on the right-canted nose now cause the nose to lean downward. The projectile is in a sort of imbalance most of this time as the various forces readjust each other and the nose actually describes a small arc in the air, known as nutation (Greek for nodding) [8].

Previously conducted work has estimated the nutation shifts the projectile tip at an angle up to α_t*=4°* from its *COG* [10] (Fig. 2). In other words, the projectile tip rotates at a certain distance, depending on αt, around $\vec{v}_{rel}$ and has an unknown position at impact. The focus on this paper is the determination of the nutation of the projectile tip has an influence in oblique impact, especially on the projectile behaviour after ricochet. If the projectile tip has a nutation in plane of impact it is stated as yaw; perpendicular as pitch. For simplification further discussed scenarios in this paper are stated as yaw. Numerical investigation supplies data about qualitative dependency of yaw angle on the projectile behaviour after it ricochets. The numerical approach is chosen as limited measurement precision makes investigation yaw angle influence under oblique impact difficult.

3 Experiments

3.1 Set-up

Oblique impact experiments were conducted launching *7.62x51 mm* projectiles at *8 mm* thick armour steel plates. The armour steel is a 350 HB hard steel. The projectile is a long hard steel core projectile, which was launched with a constant velocity of *810±15 m/s*, which was measured with a light barrier located about *500 mm* before the target. The impact was captured using high speed cameras and x-ray pictures (Fig. 1). Tested impact angles were from *0°≤θ≤70° NATO* (measured from the surface perpendicular to the projectile rotation axis).

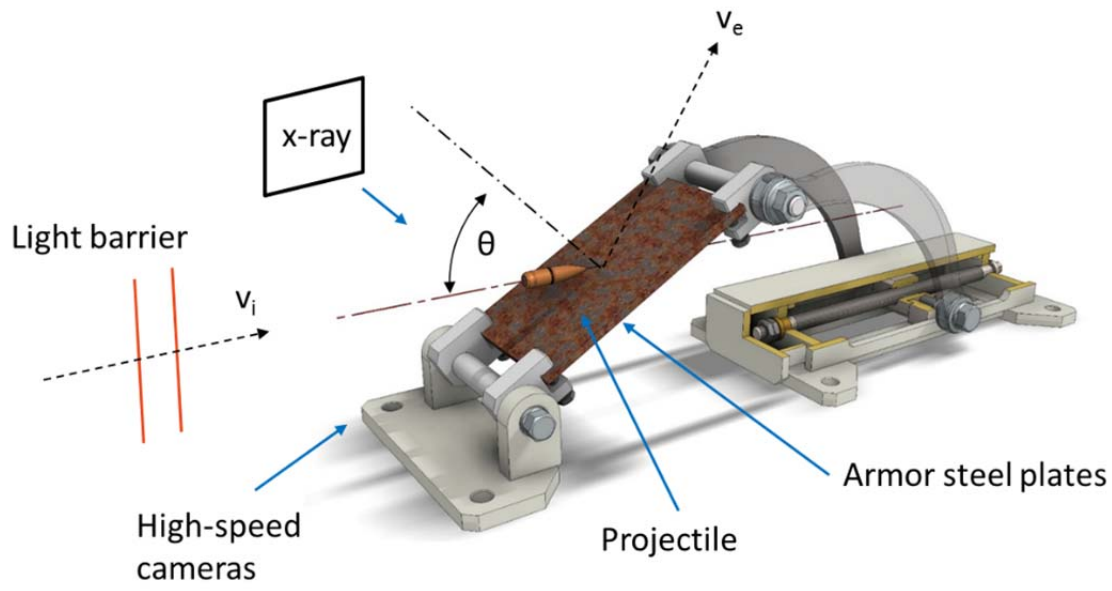

Fig. 3 Experimental set-up and measurements for oblique impact and ricochet investigation

3.2 Results

The projectile was captured on x-ray after impacting the target and showed a complex scenario after oblique impact (Fig. 4), which has been described in literature [11] [12]. For impact angle $\theta>30°$ *NATO* the projectile core penetrates the target (Fig. 4 a). For tested impact angles of $30°\leq\theta\leq60°$ *NATO*, the core ricochets and brakes (Fig. 4 b) and core and jacket fragments were retrieved (Fig. 5). The core ricochets unbroken for $\theta\geq70°$ *NATO* and keeps its integrity [3]. The critical ricochet angle is $\theta_c=30°$ *NATO* for that specific projectile on armour steel plate with a 350 HB hardness and is only true for this setting. In other words, the projectile perforated the plate for all tested impact angles $\theta<30°$ *NATO* and ricocheted for $\theta\geq30°$ *NATO*. If another projectile was used, the angle θ_c changed.

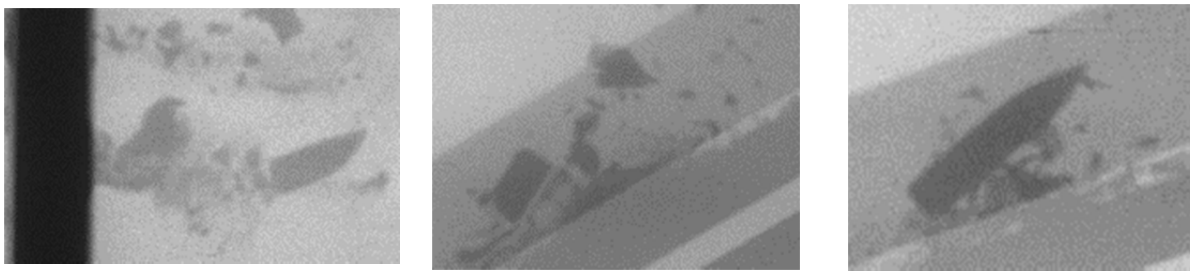

a) θ<30° penetration unbroken b) 30°≤θ≤60° ricochets broken c) θ≥70° ricochets unbroken

Fig. 4 scenario after oblique impact depending on impact angle

Previously conducted experiments [13] showed, that the projectile trajectory after ricochet stays in the plane of impact (Fig. 3). And projectile deflection from the plane was neglected. Therefore, the exit velocity was determined by measuring the projectile displacement from taken x-ray images. The images are double or triple exposed showing the projectile distribution. The time between the exposures is known and a core velocity can be estimated. For broken projectile cores, the largest visible part (Fig. 4 b) is used for the determination of the velocity. The exit velocity v_e after ricochet and a residual velocity v_a after target perforation are used as validation parameters for the numerical model.

Fig. 5 Projectile parts retrieved after oblique impact, core and jacket

4 Numerical model

4.1 Johnson-Cook material model

The numerical model was set up using solid, fully integrated brick elements in an explicit Lagrangian solver. This study investigates the core impact of the influence on ricochet, instead of a full modelled projectile [14] [15]. For such specific setting of impact of a hard steel projectile on an armour steel plate, the x-ray pictures showed that the core alone further acts on the target plate. Retrieved jacket parts lead to the assumption that the jacket spalls from the core with its first contact (Fig. 5). Core and target plate are modelled as a full three dimensional model. For later investigations on the influence of a yaw angle on ricochet, symmetry cannot be applied. For both parts, the Johnson-Cook (JC) material model [14] is applied and the Von Mises stress flow stress σ_y is given in the following equation:

$$\sigma_y = [\mathrm{A} + \mathrm{B}\bar{\varepsilon}_p^{\,\mathrm{n}}][1 + \mathrm{c}\cdot\ln(\dot{\varepsilon}^*)][1 - \mathrm{T}^{*\mathrm{m}}] \tag{1}$$

Where $\bar{\varepsilon}_p$ is effective plastic strain and $\varepsilon^* = \bar{\varepsilon}_p / \varepsilon_0$ the dimensionless plastic strain rate.

Constant *A* is the yield stress corresponding to a 0.2% offset strain; the strain hardening effects of the material are represented by constant *B* and exponent *n*. The strain rate effect is expressed through constant *C* and exponent *m* represents temperature softening of the material through homologous temperature $T^* = (T - T_0)/(T_m - T_0)$ (Table 2) [16]. *T* is the absolute temperature, T_0 is the room temperature and T_m is the melting temperature of the target material [16] [17].

4.2 Equation of state (EOS)

The JC material model needs and additional equation of state to define the material properties. The Gruneisen EOS is used for core and target:

$$p = \frac{\rho_0 c^2 \mu\left[1 + \left(1 - \frac{\gamma}{2}\right)\mu - \left(\frac{\alpha}{2}\right)\mu^2\right]}{\left[1 - (S_1 - 1)\mu - \frac{S_2\mu^2}{(\mu - 1)} - \frac{S_3\mu^3}{(\mu - 1)^2}\right]} + (\gamma + \alpha\mu)E_0 \tag{3}$$

Where E_0 is the internal energy per unit volume, intercept *c* and slope coefficients S_1, S_2, S_3, Gruneisen coefficient *γ* and volume correction *α* (Table 1). Literature provides the EOS parameters for core [19] and for the target [20].

Table 1 Gruneisen parameters for target and core

	Speed of sound	Slope			Gruneisen coefficient	Internal Energy	Relative Volume
	c[m/s]	S_1	S_2	S_3	γ	E_0[J/m³]	V_0
Target	4570	1.4	0	0	1.97	0	1
Core	4700	1.29	0	0	1.587	0	1

Both parts are in contact with a symmetric erosion contact. The mass from eroded elements is preserved during the simulation.

4.3 Target JC-parameters and failure definitions

The target was defined with the JC fracture model shown below:

$$\varepsilon^f = [D_1 + D_2 \cdot e^{D_3 \sigma^*}][1 + D_4 \cdot \ln(\dot{\varepsilon}^*)][1 + T^*] \quad (2)$$

Where ε^f is the equivalent plastic fracture strain, ε^* is the stress triaxiality factor, and D_1, D_2, D_3, D_4, and D_5 are fracture model constants [14]. Constitutive parameters for armour steel have been determined from tensile tests [18] and are summarised in Table 2.

Table 2 Constitutive Model constants for target plate

Elastic constants and density			Yield stress and strain hardening			Strain rate hardening	
E[MPa]	v	ρ[kg/m³]	A[MPa]	B[MPa]	n	$\dot{\varepsilon}_0$[s⁻¹]	C
$2.1 \cdot 10^5$	0.33	7840	844	622	0.164	10^{-3}	0.01

Adiabatic heating and temperature softening				Fracture strain constants				
C_p[J/kgK]	T_m[K]	T_0[K]	m	D_1	D_2	D_3	D_4	D_5
450	1800	273	1.058	0	2.12	-1.45	0	-0.68

Solid elements are defined to fail with $\sigma_1 \geq \sigma_{max}$, with σ_1 is the maximum principal stress and σ_{max} is the principal stress at failure. The additional core breaking seen in the experiments (Fig. 4b) is not taken into account, because the aim is the dependency of the yaw angle on the projectile core behaviour under oblique impact and especially on ricochet for $\theta \geq \theta_c (=30°\ NATO)$. If the core breaks, additional definition in failure needs to be made, which would compromise a comparison with an unbroken scenario such as shown as impossible in Fig. 4.

4.4 Core JC-parameters

The core was hard steel with parameter settings determined by quasi-static compression tests. Further, material parameters, which have not been determined, were taken from literature [17]. For the projectile, no additional failure criterion was defined.

Table 3 Constitutive Model constants for core

Elastic constants and density			Yield stress and strain hardening			Strain rate hardening	
E[MPa]	v	ρ[kg/m³]	A[MPa]	B[MPa]	n	$\dot{\varepsilon}_0$[s⁻¹]	C
$2.1 \cdot 10^5$	0.34	7840	500	10^5	0.2	10^{-3}	0.008

Adiabatic heating and temperature softening				Fracture strain constants				
C_p[J/kgK]	T_m[K]	T_0[K]	m	D_1	D_2	D_3	D_4	D_5
475	1800	273	1.0	no fracture				

5 Numerical model validation

Every second simulation is shown and discussed in order to represent of the full oblique impact scenario. Beginning at an impact angle *θ =10° NATO*, the simulation is validated for the penetration case (Fig. 4 a). The cases for *30°*and *50° NATO* represent the ricochet scenario with a broken core and simulations are compared with experiments (Fig. 4 b). The impact angle *θ =70° NATO* is validated for a ricochet case with unbroken core (Fig. 4 c). Two parameters where chosen for validation, the target damage signature and the core velocity after impact.

5.1 Target damage and failure

5.1.1 Penetration

The impact angle of *θ=10° NATO* shows the perforation case (Fig. 6). The projectile penetrates the target which is shown at *t=10µs* (Fig. 6 a), moves through the target thickness (Fig. 6 b) until it fully exits the steel plate (Fig. 6 c). The smallest elements from the decreasing mesh size on the projectile tip are eroded. The projectile keeps its integrity which agrees with experimental results (Fig. 4 a)

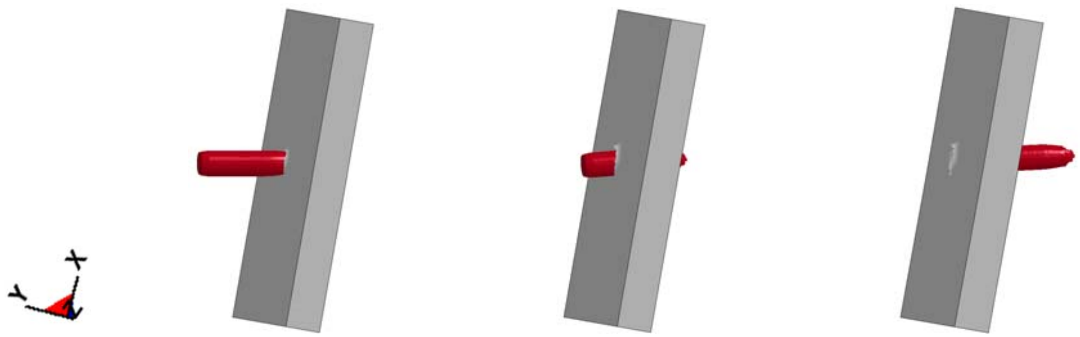

a) t=10µs b) t=30µs c) t=50µs

Fig. 6 Hard core perforates steel target at an angle θ =10° NATO

The case (Fig. 6) for a *θ =10° NATO* impact can be used to verify the numerical model. The projectile does not break and therefore the damage criteria in the target material and the residual velocity v_a after perforation (Fig. 11) can be compared to numerical results. For comparison were the size and shape of the hole created on strike (Fig. 7 a) and back face (Fig. 7 b) of the steel plate.

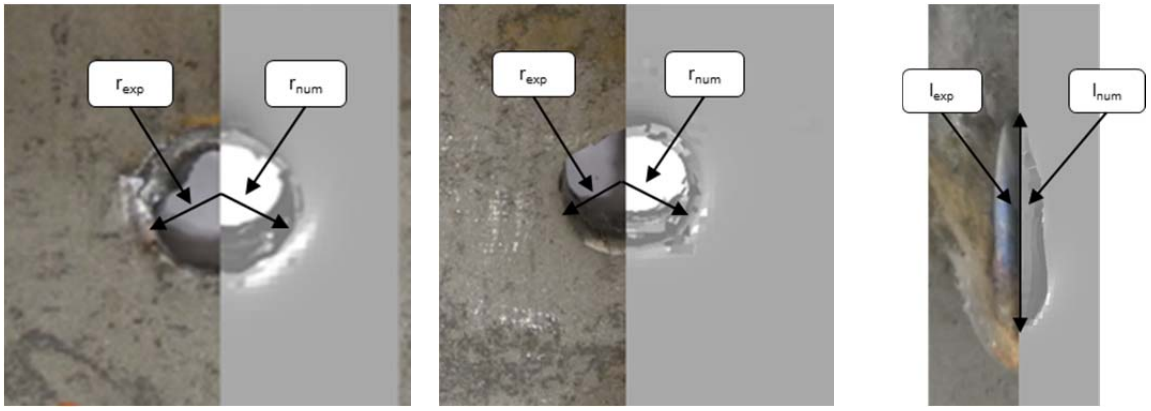

a) Strike face for θ =10° b) Back face for θ =10° c) Strike face for θ =70°

Fig. 7 Strike and back face deformation, experimental and numerical comparison of target deformation

The numerical simulations were compared to the experimental results in the prediction of the target deformation and fracture. The hole, where the core penetrated the target, was represented qualitatively very well in its shape by the numerical simulation. Quantitatively, it was observed, that the numerical simulation predicted a radius r_{num} of *4 mm*, whereas in reality the radius r_{exp} was *4.5-5 mm* (Fig. 7). The reason for this occurrence is possibly the assumption of the impact of the core only instead the full modelled projectile. Therefore, it may be sufficient to assume the core only during oblique impact, as the brass jacket seems to spall off upon impact, yet for the target deformation that assumption may not be applicable.

5.1.2 Ricochet with broken core

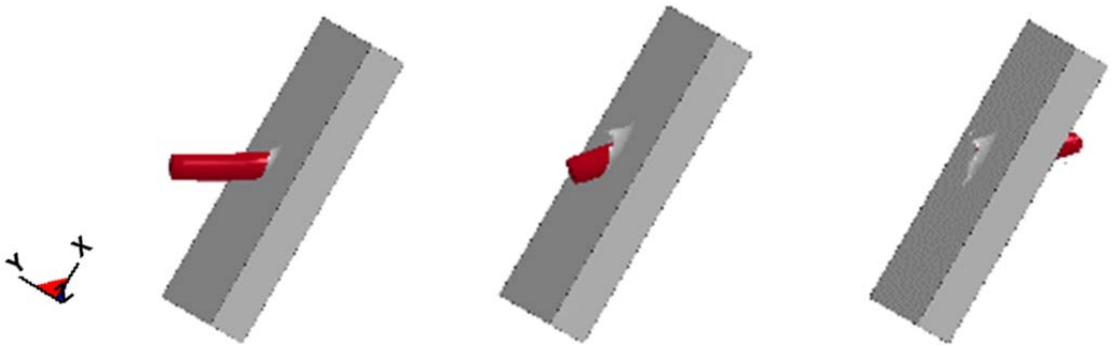

a) t=10µs b) t=30µs c) t=50µs

Fig. 8 Hard core penetrates steel target at an angle θ =30° NATO

Fig. 8 and Fig. 9 show penetration over prediction of the numerical model, caused by the neglected core material failure. At an impact angle of *θ =30° NATO*, the numerical result show penetration, which under predicts the ricochet occurrence. With increase of *θ* (Fig. 9) the numerical model shows ricochet. As previously stated, the core breaking is not taken into account and is in focus of additional studies.

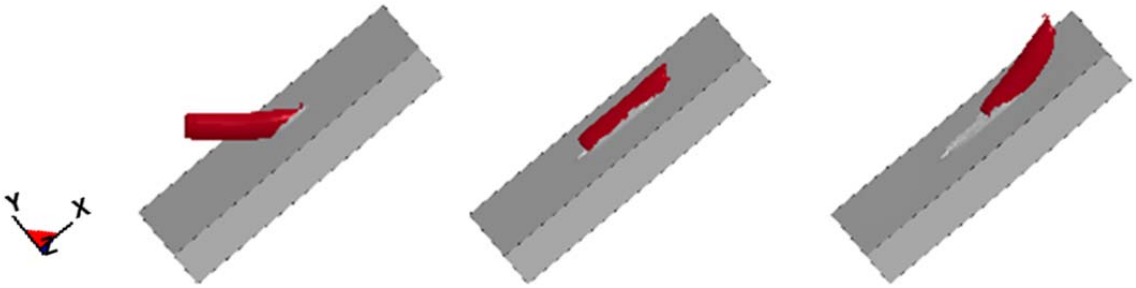

a) t=10µs b) t=30µs c) t=50µs

Fig. 9 Hard core ricochets from steel target at an angle θ =50° NATO

5.1.3 Ricochet with unbroken core

The ricochet case shows the core at an impact angle of *θ =70° NATO* (Fig. 10). At first contact, shown at *t=10µs* (Fig. 10 a), the numerical model over predicts the elastic core behaviour. This is due to the chosen core material parameters (Table 3). These material parameters where compared to other existing representations of projectile cores [21]. Although having a tendency to an elastic over prediction (Fig. 10 a, b), this core representation showed the most stabile behaviour throughout all ricochet simulations. The target damage after ricochet (Fig. 10 c) was compared to experiments (Fig. 7 c). The numerical representation of length l_{num} agrees with experimental length l_{exp}. The penetration depth is over predicted in the numerical model with about *0.5 mm*. However, the overall numerical target damage representation agrees with the experiment.

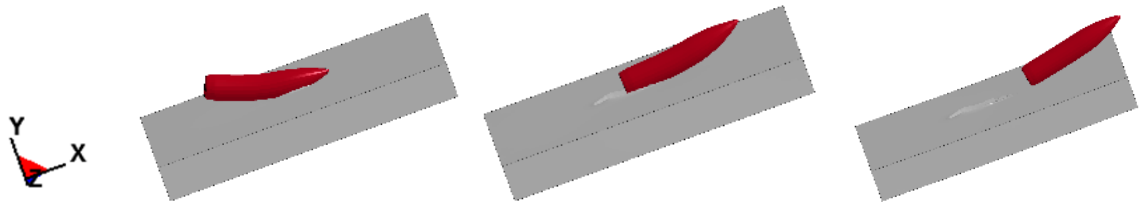

a) t=10µs b) t=30µs c) t=50µs

Fig. 10 Hard core ricochets from steel target at an angle θ =70° NATO

5.2 Core velocity validation

The core velocity, after impact on the target plate, is compared between numerical and experimental results. Here, two cases are distinguished. First, the residual core velocity v_a after perforation (Fig. 11), where the core went through the target thickness and exits the back face (Fig. 7 b). Second, the core velocity after ricochet from the target is compared which is stated as exit velocity v_e (Fig. 12).

5.2.1 Penetration

Figure Fig. 11 shows the residual velocity v_a of the projectile core plotted from the numerical simulation (Fig. 11 a). For tested impact angles of *θ<30° NATO*, target perforation occurred. The results are compared to measured velocity from the x-ray pictures (Fig. 4). The numerical model agrees in the prediction of v_a with experiments (Fig. 11 b).

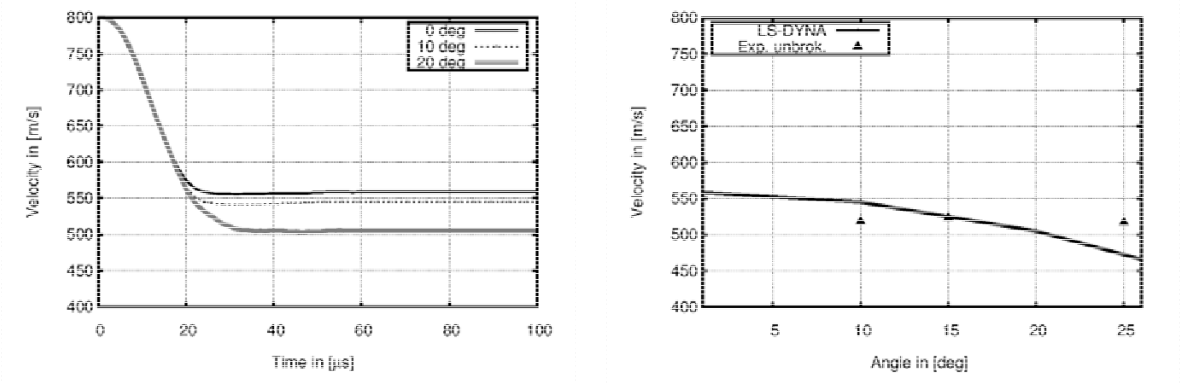

a) Residual velocity v_a after perforation b) Comparison v_a to experiments

Fig. 11 Residual core velocity v_a depending on impact angle

5.2.2 Ricochet

At tested angles of *θ≥ 30° NATO*, projectile core ricochet occurs. However, for angles of *30°≤θ<50° NATO*, the projectile core breaking is so severe, that a velocity measurement from the x-ray pictures is hardly possible. For impact angles of *θ≥50° NATO*, the projectile velocity after ricochet v_e can be measured and is compared to the numerical simulations (Fig. 12). The numerical prediction agrees especially for *θ=70° NATO*, where, except one time, no projectile core breaking occurred. The reason is that if a core breaks, smaller pieces, have a higher velocity than the unbroken core.

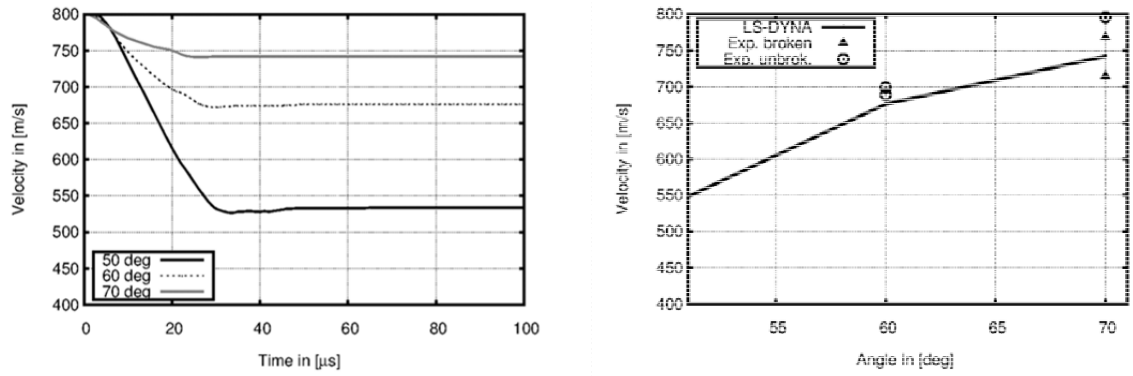

a) Exit velocity v_e after ricochet b) Comparison v_e to experiments

Fig. 12 Exit core velocity v_e depending on impact angle

6 Numerical yaw angle model

6.1 Case studies

This model was further modified, involving the yaw angle. The yaw angle was represented numerically by rotating the core around its *COG* with α_t=4° and three positions were chosen to represent the most extreme influences of α_t. Firstly, the core is counter-clockwise rotated from its initial position around z-axis; defining it as position *A* (Fig. 13 a). The position *C* is defined by clockwise core rotation around z-axis (Fig. 13 c). *B* is core position by a rotation around x-axis. This specific configuration *B* is also known as pitch angle. As stated earlier, it will be referred to as yaw angle for simplification. The initial position is stated as *O*, which was set for the validation (Fig. 13).

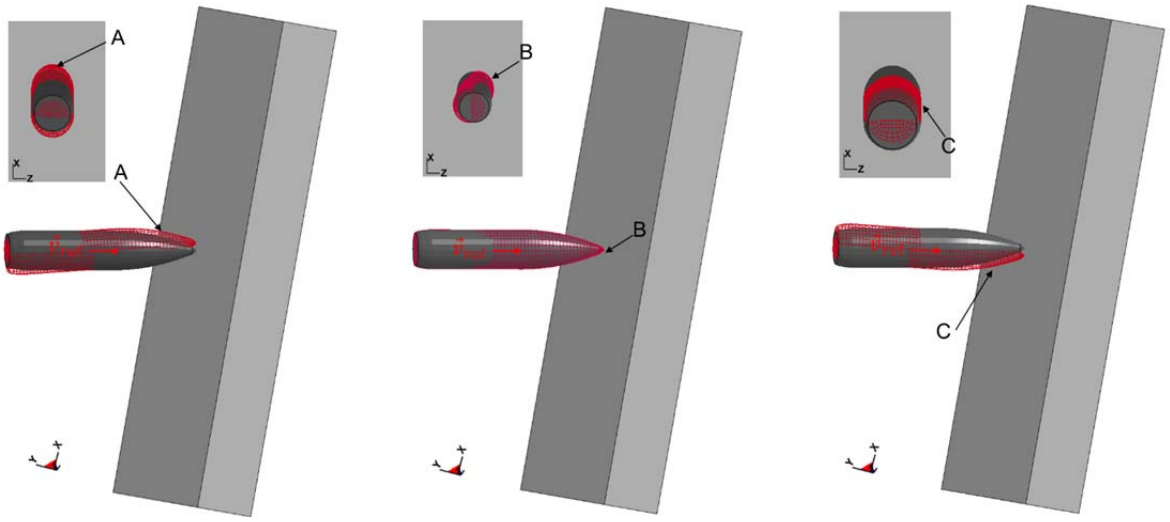

a) Case A b) Case B c) Case C

Fig. 13 Representative test cases shown at θ =70° NATO for the yaw angle (with case B also stated as yaw angle)

6.2 Results and discussion

When a projectile or core perforates an inclined plate, the thickness d_{los} in the line of sight is larger compared to normal plate thickness *d* (Fig. 14). Depending on the impact angle θ (in NATO degrees); as larger the angle, as thicker is the plate:

$$d_{los} = \frac{d}{\cos(\theta)} \tag{4}$$

The trajectory through the material changes for each test case and therefore the thickness which needs to be penetrated (Fig. 14).

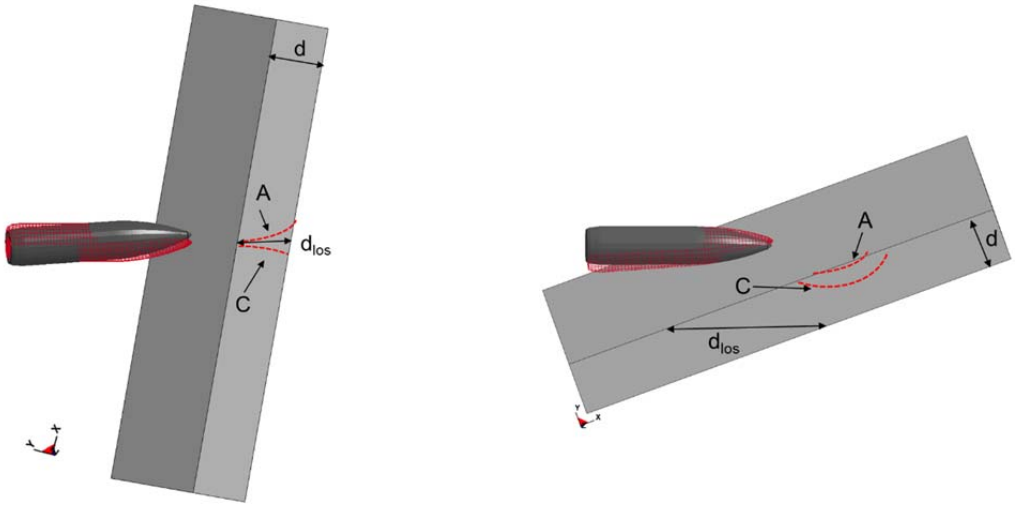

a) Perforation b) Ricochet

Fig. 14 Core trajectory through material depending on yaw angle

6.2.1 Penetration

The impact angle *θ=10° NATO* represents influence of yaw angle for tested perforation cases (Fig 11). Case *A* has the lowest deflection in vertical direction, whereas *C* has the highest and the *B* shows little influence compared to the initial state *O* (Fig. 15 a). When the core for case *C* gets deflected in y-direction, it passes through a lower thickness *d* than $d_{los.}$ This means that case *C* experiences a shorter negative acceleration and therefore has a higher residual velocity (Fig. 15 b). Case *A*, which passes thought a longer thickness compared to $d_{los,}$ has the slowest v_a.

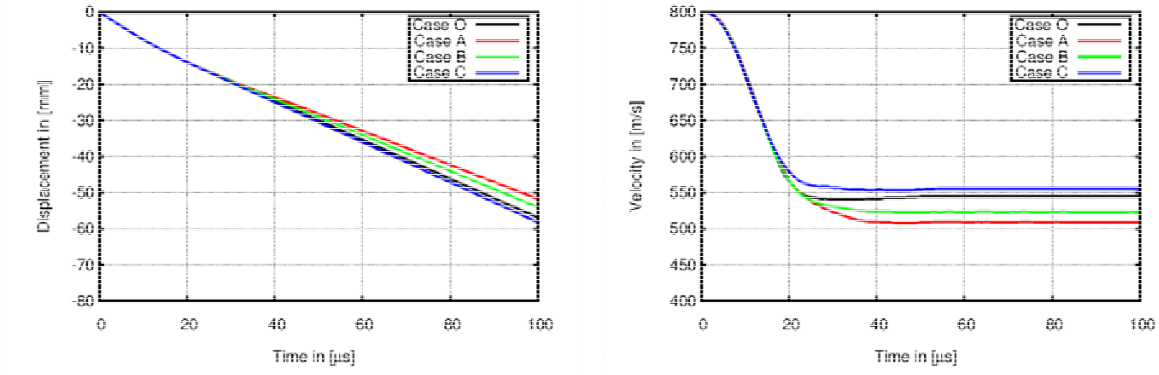

a) Displacement at θ=10° NATO b) Velocity at θ=10° NATO

Fig. 15 Vertical core displacement and velocity as a function of time for θ =10° NATO for tested yaw angle cases

6.2.2 *Ricochet with broken core*

At the angle *θ=40° NATO*, the numerical simulation shows a significant influence of the yaw angle on ricochet. Case *C* showed perforation. In case *O* and *B*, the core stuck inside the plate, and *B* showed ricochet. Only ricochet was observed experimentally for this specific impact angle, as in reality the core broke without exception under that impact angle. However, such case visualised, that the influence of yaw angle is significant under impact angles which are at the boundary angle θ_c between perforation and ricochet. Therefore, the consideration of projectile yaw angle may be important for further planned experiments on softer targets, where no core breaking occurs.

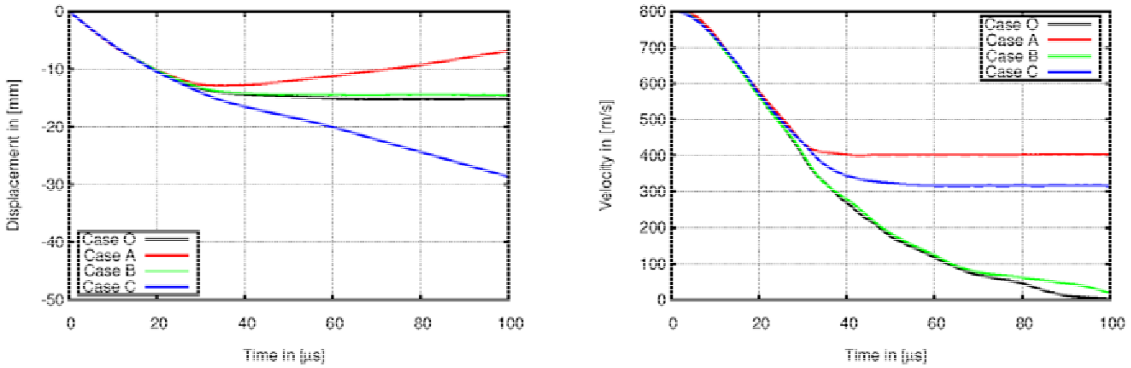

a) Displacement at θ=40° NATO b) Velocity at θ=40° NATO

Fig. 16 Vertical core displacement and velocity as a function of time for θ =40° NATO for tested yaw angle cases

6.2.3 *Ricochet with unbroken core*

For the ricochet case in Fig. 17, case *A* also has the largest deflection in negative y-direction, however here it causes the core to penetrate deeper in the material and therefore has a longer contact with the target causing the lowest exit velocity. It is also noticeable that as further away from the boundary angle between perforation and ricochet, as less influence had the yaw angle α_t had on the core trajectory.

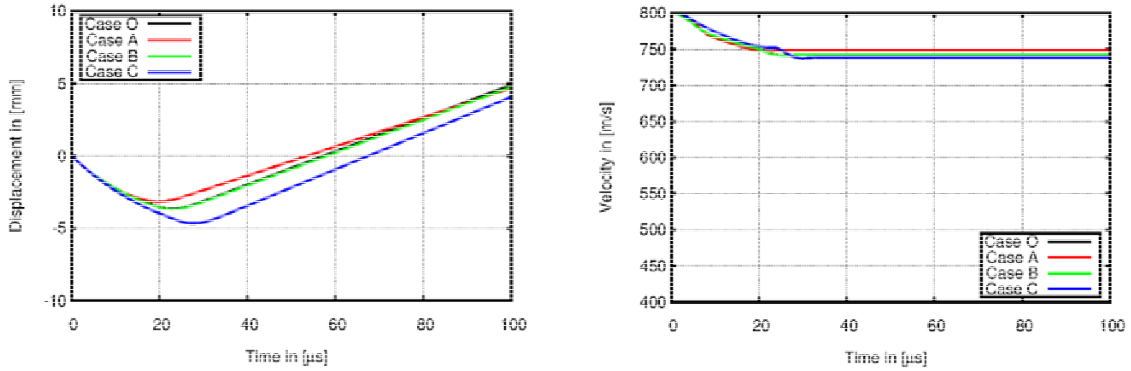

a) Displacement at θ=70° NATO b) Velocity at θ=70° NATO

Fig. 17 Vertical core displacement and velocity as a function of time for θ =70° NATO for tested yaw angle cases

7 Summary

This study gives a qualitative understanding of the dependency of the yaw angle α_t under oblique impact. The set-up was a spin stabilised hard core projectile impacting armour steel plates under different impact angles. Core velocity and the critical angle, where ricochet occurred, were of interest. Numerical simulation could be successfully validated with experimental results. The validated simulation was further used for investigating the yaw angle on the ricochet scenario. It is shown, that as closer the impact occurs to the critical angle, as larger was the influence of the yaw angle. The results provide ground work for further numerical investigations into the influence of different, experimentally hard to determine, parameters and their influence on projectile trajectory after oblique impact.

8 Literature

[1] Collins S., “Challenges of Urban Cities in 2035 - NATO Needs to Act Today to Prepare the Alliance for the Future“, Available: http://www.act.nato.int/volume-4-urbanization-the-future-challenge-for-nato, 2015.
[2] Piper P., “A Concept for Future Military Operations on Urbanized Terrain“, Department of the Navy Marine Corps Combat Development Command, Quantico, VA, 1997.
[3] Jauhari M., “Bullet Ricochet from Metal Plates“, J. of Criminal law and criminology, 60(3), 1970, pp. 387-94.
[4] Gibbon J., “The Artillerist's Manual”, New York: Baker & Godwin printers, 1860.
[5] Wood J., “The Gun Digest Book of Firearms Assembly/Disassembly Part IV - Centerfire Rifles”, Krause Publications, 2003.
[6] Shideler D., “Gun Digest Book of Classic Combat Handguns”, Krause Publications, 2011.
[7] McCoy R., “Modern Exterior Ballistics the Launch and Flight Dynamics of Symmetric Projectiles”, Schiffer Publishing, 1999.
[8] Jurens B., “Projectile Dynamics”, NavWebs, 1999.
[9] Litz B., “Gyroscopic (spin) Drift and Coriolis Effect“, Applied Ballistics, 2008.
[10] Wellige B. and Wollmann E., “Untersuchungen zum Schutzvermögen von an ihrer Oberfläche gehärteten Blechen aus Panzerstahl“, ISL - NI 903/2003.
[11] Rosenberg Z. and Dekel L., „Terminal Ballistics“, Springer-Verlag, 2012
[12] Recht R. and Ipson T., ”The dynamics of terminal ballistics“, Denver Research Institute No. AD 274128, 1962.
[13] Seidl M. and Wolf. T., “Numerical and experimental investigations on ricochet of 7.62mm NATO projectiles against aluminium targets“, LWAG, Grenoble, France, 2016.
[14] Johnson G. and Cook W., „A constitutive model and data for metals subjected to large strains, high strain rates and high temperatures“, 7th ISB, Netherlands, 1983.
[15] Peroni L. et al, “Mechanical properties at high strain-rate of lead core and brass jacket of a NATO 7.62 mm ball bullet“, EPJ Web of Conferences, 26(01060), 2012, pp. 1-8.
[16] Brar N. et al, “Constitutive Model Constants for Al7075T651 and Al7075T6“, AIP Conference Proceedings, 2009, pp. 1195:945.
[17] Bovrik T. et al, “Perforation of 12 mm thick steel plates by 20 mm diameter projectiles with flat, hemispherical and conical noses“, Int. J. Impact Eng., 27(1), 2002, pp. 27-34.
[18] Gailly B., « Etude du comportement dynamique et de la rupture de trais Aciers a blindage », Bourges, France: PhD Thesis, 1997.
[19] Favorsky V. et al, “Experimental-Numerical Study of Inclined Impact in Al7075-T7351 Tagets by 0.3" AP Projectiles,” 26th ISB, US, 2011.
[20] Nilsson M., “Constitutive Model for Armox 500T and Armox 600T at Low and Medium Strain Rates“, Swedish Defence Research Agency, 2003.
[21] Kilic N. et al, “Ballistic behaviour of high hardness perforated armour plates against 7.62 mm armour piercing projectile“, Materials & Design, 63, 2014, pp. 427-38.